Journal of Superconductivity and Novel Magnetism
https://doi.org/10.1007/s10948-023-06663-9

ORIGINAL PAPER

Probing Evolution of the Flux-Pinning Landscape in REBCO Coated Conductors Caused by Gamma Irradiation Using DC and AC Magnetometry: A Novel Approach to Tokamak Magnet Material Development

Holly Jane Campbell[1] · **Yifei Zhang**[2] · **Toru Fukushima**[2]

Received: 18 August 2023 / Accepted: 29 November 2023

Abstract
Optimisation of REBCO coated conductor tapes specifically for use in nuclear fusion will help improve the magnet component lifetimes in future tokamak reactor power plants. The focus of this work was exploration of a novel approach to irradiation studies on REBCO tapes, utilising multiple magnetic measurements to probe evolution of the REBCO flux-pinning landscape more deeply than reported in other studies, for the purpose of identifying primary limiting factors affecting performance. Gamma irradiation experiments were conducted, and pre-/post-irradiation results from DC and AC magnetic measurements using a Physical Property Measurement System (PPMS) are discussed. Magnetisation critical current density (J_c) decreased in all samples with increasing dose, except for the silver overlayer-only samples which did not contain artificial pinning centres (APCs), where J_c increased with dose. Removal of the copper stabiliser coupled with the presence of APCs allowed gamma irradiation to induce pinning force maximum peak shifts, from above 14 T before irradiation to below 9 T afterwards. Flux creep rate varied with the evolving pinning landscape, and the degree of J_c degradation directly correlated with creep rate fluctuations post-irradiation. Changes in critical temperature and diamagnetic saturation also corresponded with changes in J_c and flux creep rate. The major conclusion from this study was that minimisation of flux creep rate is the key to maintenance of performance under fusion-relevant operating conditions. Flux creep manifests as problematic AC losses in all high-temperature superconducting machines; therefore, future work will focus on reduction/prevention of the phenomenon to enhance longevity of performance in any application.

Keywords REBCO · Coated conductors · Fusion magnets · Gamma irradiation · Magnetometry analysis

1 Introduction

The favourable properties of REBCO coated conductor tapes and the well-established production methods have brought these tapes to the forefront of tokamak fusion research [1, 2]. Magnet materials experience harsh conditions inside a tokamak: high magnetic fields, high input currents, and intense neutron and gamma radiation [3]. Under these conditions, magnet longevity is an issue due to short expected lifetimes, high costs associated with replacement, and supply chain concerns.

In the literature, it is established that under high applied magnetic fields, fast neutrons can enhance critical current density (J_c) via the introduction of nm-scale collision cascades up to a maximum fluence, often around $1–2 \times 10^{22}$ neutrons/m^2 above 10 T, before degradation when further exposed [4–6]. The onset of degradation occurs at lower fluences when tape REBCO layers have a higher pristine sample defect density, due to the presence of artificial pinning centres (APCs) [7]. Literature on the effects of gamma rays is inconclusive [8–10].

For optimisation of REBCO tapes in fusion applications, performance testing under fusion-relevant operating conditions (20 K and very high magnetic fields above 10 T)

✉ Holly Jane Campbell
holly.campbell@ukaea.uk

[1] UKAEA (United Kingdom Atomic Energy Authority), Culham Science Centre, Abingdon, Oxfordshire OX14 3DB, UK

[2] SuperPower Inc., 21 Airport Road, Glenville, NY 12302, USA

Published online: 15 December 2023

before and after irradiation is required. Critical parameters in REBCO are very sensitive to irradiation [11], and the evolution of functionality in a tape is dependent on applied temperature and field. Magnetometry probes the flux-pinning landscape, providing insight into screening capability and flux dynamics [12]. The combination of multiple magnetic property analyses will improve our understanding of the underlying mechanisms behind irradiation-induced performance evolution in REBCO tapes, with the aim of this work being identification of the key performance-limiting factors at low temperatures and high fields.

There is extensive literature on the effects of irradiation on REBCO functional properties [4–11, 13–23]. Therefore, the purpose of this study was to take a different direction, using the knowledgebase acquired through previous REBCO irradiation work, but moving away from solely improving mechanistic understanding of irradiation effects by beginning to address the irradiation-induced issues. This study was intended as a relatively quick piece of work to evaluate the universal issues affecting degradation of performance in any REBCO tape sample under fusion-relevant conditions, acting as a compass pointing towards the most urgent direction necessary for fusion-tape development.

Gamma irradiation was chosen in this study because gamma rays are expected to bombard tokamak magnets, yet gamma effects on REBCO tapes are poorly understood. Pre-/post-irradiation magnetic testing comprised of DC moment versus field hysteresis loop, DC magnetic relaxation, and AC susceptibility measurements.

The results from magnetic testing on gamma irradiated tape samples are discussed. Overarching themes affecting degradation of performance after irradiation, irrespective of pristine flux-pinning landscape in the tape, and the connections between different types of measurement data are also explored. This work demonstrates the complex relationship between pristine pinning landscape and evolution of performance under irradiation.

2 Methods

2.1 Samples and Irradiation

The tapes examined in this work were 3 SuperPower 4-mm wide SCS4050 GdYBCO samples (Fig. 1).

Each had 0, 7.5, or 15% additional Zr by weight within the REBCO layer for $BaZrO_3$ nanocolumn APC generation, and sections of the tapes were chemically etched after receipt to remove the Cu stabiliser prior to irradiation, providing analogous Ag-only samples (in total, 6 samples for post-irradiation analysis).

Gamma irradiation experiments were carried out at the Dalton Cumbrian Facility. The REBCO tape samples were irradiated with Co-60 gamma rays up to 1 kGy and 1 MGy doses. The irradiation angle was parallel to the REBCO *c*-axis. With the assumption that damage introduced to the microstructure and/or electronic structure is isotropic, it is also assumed that the angle of irradiation does not influence post-irradiation changes in functionality [5].

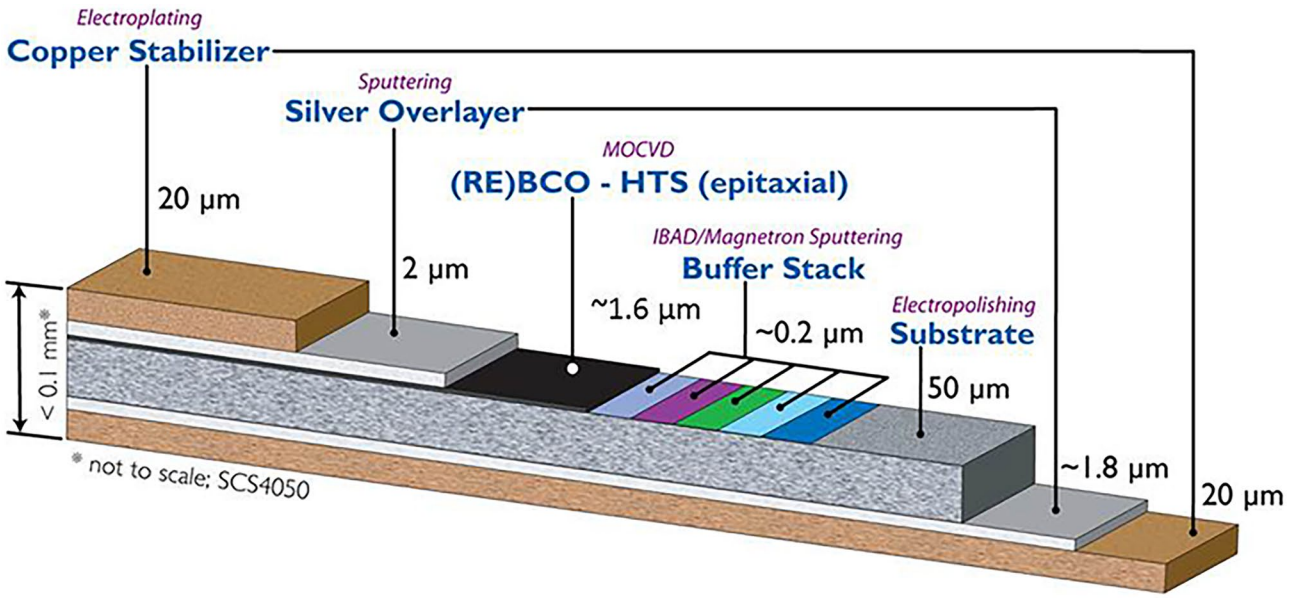

Fig. 1 Schematic diagram of a SuperPower SCS4050 REBCO coated conductor tape [24]

2.2 Measurement Setup

Magnetometry measurements were conducted on the tape samples using the AC magnetic susceptibility (ACMS) operational mode of the Quantum Design PPMS® DynaCool™ Physical Property Measurement System (PPMS) at the UKAEA Materials Research Facility (MRF). The PPMS in the MRF is intended for characterisation of functional properties in radioactive/irradiated materials. For all measurements, 3-mm disk samples were cut from the tapes prior to irradiation (and for the Ag-only samples, after chemical etching of the Cu stabiliser) using a SPI Supplies #17,001-AB precision TEM disk punch, and magnetic fields were applied parallel to the REBCO *c*-axis.

During AC susceptibility measurements, a 0.001 T AC drive field with a frequency of 777 Hz was also applied along with the DC field. The applied temperature (20 K) in the DC measurements and applied field (14 T) in the AC (and DC magnetic relaxation) measurements were chosen to simulate fusion-operating conditions most accurately. The magnetometry measurements thus probed gamma-induced changes to the flux-pinning landscape within the REBCO *ab*-axis under these conditions.

Different samples from each tape were used for pre-/post-irradiation magnetometry examination, with analysis based on the assumption of REBCO thickness uniformity. To verify that measured post-irradiation changes were induced by the gamma rays, repeat measurements were conducted on 3 non-irradiated samples from the 7.5% tape, and the data were collated in Figs. 2, 3, 4, 5, and 6 and Tables 1 and 2. Calculated J_c values for the repeat samples were higher than in the pre-irradiation sample from the same tape shown in Figs. 8 and 11; the samples in Figs. 2, 3, 4, 5, and 6 were measured ~ 10 months later after a renewed ACMS mode calibration.

Pre-irradiation, 3 tape samples were analysed: 1 sample from each of the parent tapes. Post-irradiation, 12 tape samples were analysed: 4 samples from each of the parent tapes; 1 Cu-stabilised and 1 Ag-only sample at both 1 kGy and 1 MGy gamma doses.

All profiles for each specific sample were generated from measurements on that same individual sample in a single experimental sequence, and the consistent trends in functional property changes seen across all the irradiated samples will be discussed in Sect. 3.

2.3 Data Analysis Calculations

Magnetisation-J_c values were calculated from DC magnetic moment versus applied magnetic field hysteresis loops using Bean's critical state model for a thin film: $J_c = (15 \times \Delta m)/(V \times r)$, where Δm is the magnetic moment difference, V is REBCO layer volume, and r is the sample radius (Figs. 2 and 3) [25]. Overall pinning force values (F_p) were calculated using the following equation: $F_p = J_c \times B$, where B is magnetic field (Fig. 4). Flux creep rates were calculated from DC magnetic relaxation measurements using the $(-d \ln M)/(d \ln t)$ line of best fit gradient, where M is the volume magnetisation and t is time (Fig. 5) [26, 27].

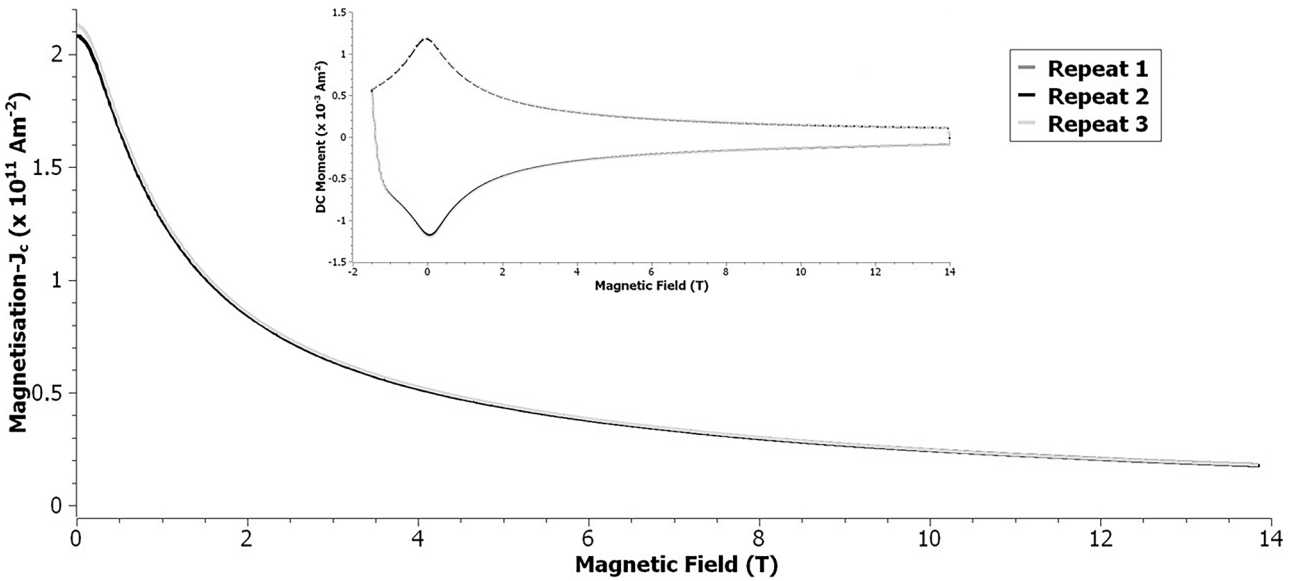

Fig. 2 Magnetisation critical current density versus magnetic field strength for 3 repeat samples of the 7.5% Zr tape—J_c values calculated at 20 K using the inset DC moment versus field hysteresis loops

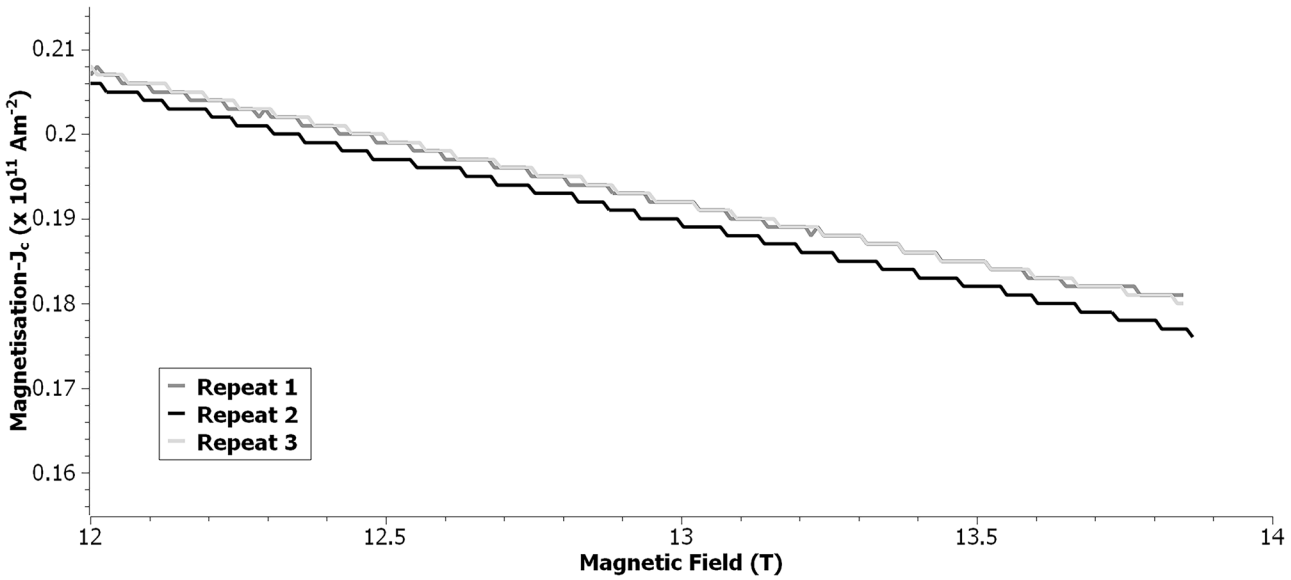

Fig. 3 High field zoom-in of magnetisation critical current density versus magnetic field strength for 3 repeat samples of the 7.5% Zr tape—J_c values calculated at 20 K

3 Results and Discussion

3.1 DC Magnetic Data

3.1.1 Magnetisation Critical Current Density

After gamma irradiation, there were patterns in J_c changes for each tape. Error values for the calculated J_c values were assumed to be the same as in Table 1.

Figures 7, 8, 9, 10, 11, and 12 present the gamma-induced changes in J_c across all 3 tapes. For the 0% tape, J_c decreased with increasing dose in the Cu-stabilised samples whilst J_c increased in the Ag-only samples.

For the APC-containing tapes, J_c decreased in all 4 irradiated samples, to a greater extent in the Ag-only samples. The post-irradiation reduction in J_c was larger in the 15% tape relative to the 7.5% tape. Interestingly, for the 15% tape, J_c in the Cu-stabilised samples increased between 1 kGy and 1 MGy irradiation;

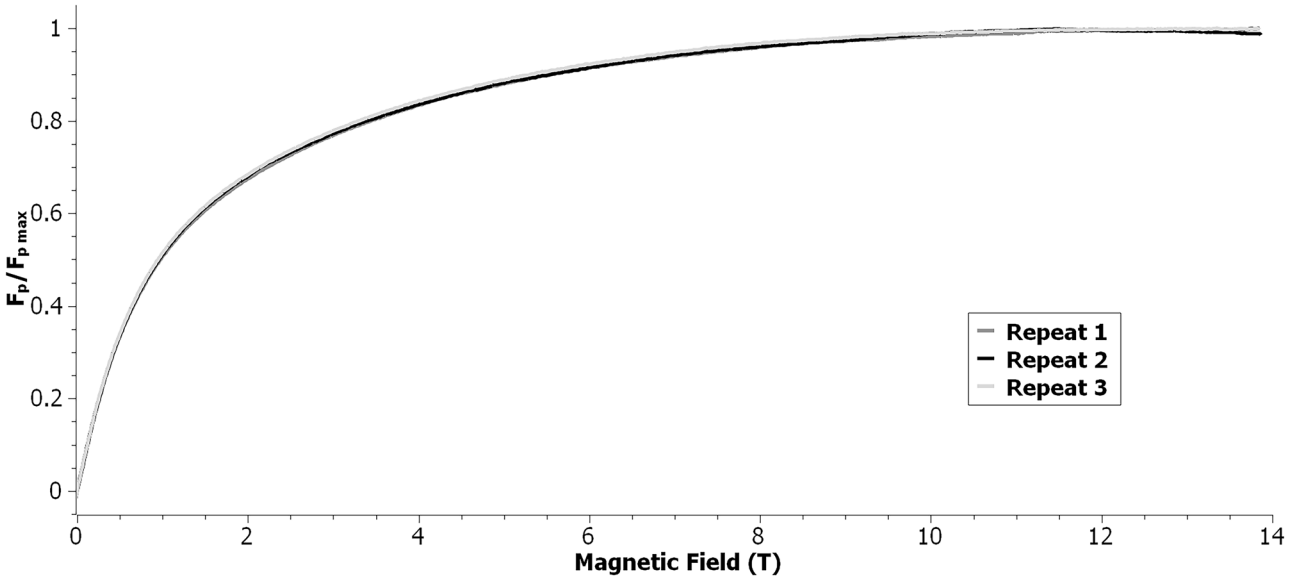

Fig. 4 Normalised pinning force versus magnetic field strength for 3 repeat samples of the 7.5% Zr tape—F_p values calculated at 20 K

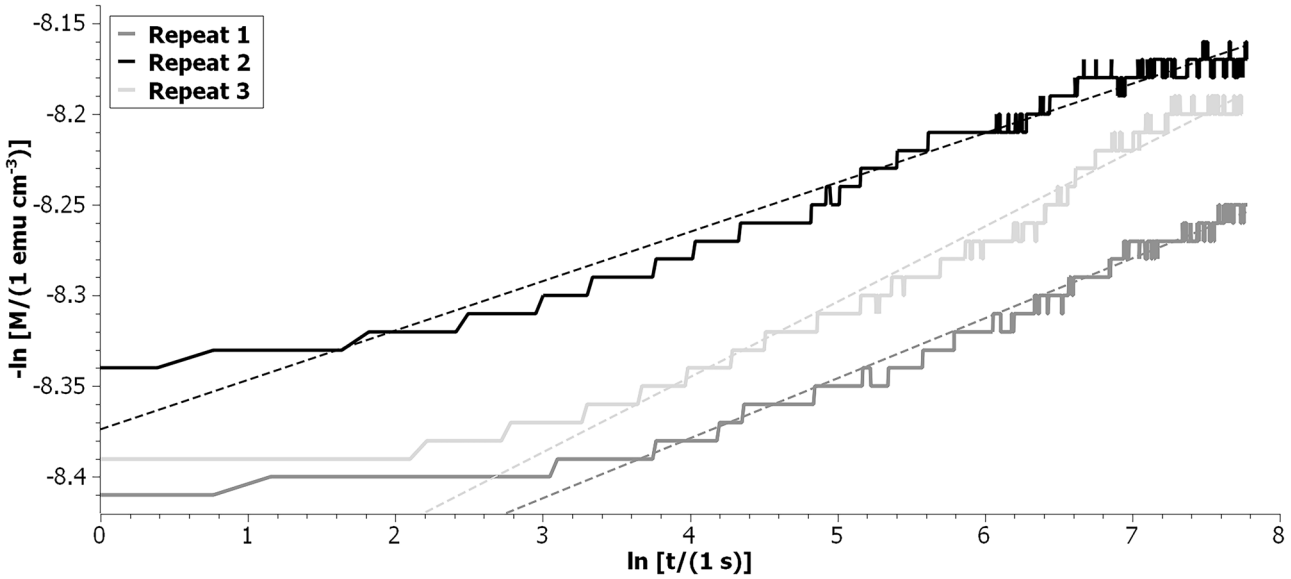

Fig. 5 Natural logarithm of volume magnetisation versus natural logarithm of time for 3 repeat samples of the 7.5% Zr tape at 20 K and 14 T—flux creep rates equal the line of best fit gradient (dashed lines)

in the 7.5% Cu-stabilised and all 4 APC Ag-only samples, J_c decreased between 1 kGy and 1 MGy irradiation at very high fields (below 10 T, J_c in the 7.5% Cu-stabilised samples was higher after 1 MGy, but above 13 T, J_c was lower after 1 MGy).

In the upcoming sections, the underlying mechanisms behind these changes in J_c will be investigated.

3.1.2 Overall Pinning Force

To supplement the J_c analysis, overall F_p versus field profiles were calculated. A theory that will be discussed in this section is the idea of F_p profiles probing changes in dominant pinning centre within the overall flux-pinning landscape

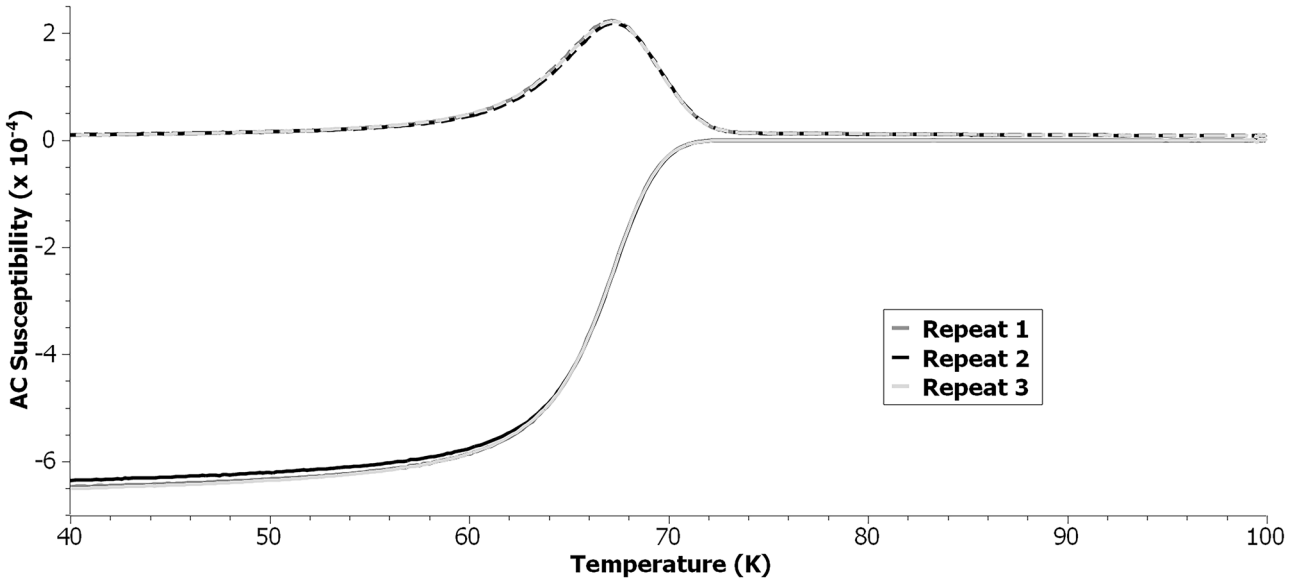

Fig. 6 AC susceptibility versus temperature for 3 repeat samples of the 7.5% Zr tape—susceptibility values at 14 T

Table 1 Magnetisation critical current density values calculated at 20 K and 13.85 T for 3 repeat samples of the 7.5% Zr tape—related statistical parameters are also included

Repeat sample	J_c (Am^{-2})
1	1.81E + 10
2	1.77E + 10
3	1.80E + 10
	Mean value—1.79E + 10
	Margin of error—2.58E + 08
	Confidence level—99%
	Standard deviation—1.73E + 08

Table 2 Flux creep rates calculated at 20 K and 14 T for 3 repeat samples of the 7.5% Zr tape—related statistical parameters are also included

Repeat sample	Flux creep rate
1	3.3E-02
2	2.7E-02
3	4.0E-02
	Mean value—3.33E-02
	Margin of error—7.90E-03
	Confidence level—99%
	Standard deviation—5.31E-03

via shifts in the field strength at which $F_{p\,max}$ was observed pre-versus post-irradiation. For pristine REBCO, the field strength corresponding to $F_{p\,max}$ is known to signify the dominant pinning centre, and the plateau of the profile curve slope indicates the transition between strong core-interaction flux-pinning to weak elastic vortex-vortex interactions: in work by Galstyan et al. on pristine REBCO thick films, it was concluded that at low temperatures below 30 K and at high fields above 8 T, there was a transition from strong correlated pinning by the $BaZrO_3$ nanocolumn APCs present in the produced films to weak uncorrelated pinning by Frenkel pair point defects [28]. Profiles for the pre-irradiation APC-containing samples similarly plateau at ~ 8 T.

In pristine APC-containing tapes, APCs act as the dominant pinning centre in a landscape also occupied by other microstructural defects of varying pinning strengths (in the order of APCs > nm-sized defects > point defects) [27]. Transitions in the overall pinning mechanism dominating the landscape, from strong individual pinning by nm-scale microstructural defects (such as APCs, grain boundaries, and dislocations) to weak collective pinning by point defects, are also caused by the reduction in *ab*-axis coherence length with increasing radiation dose [13, 27, 29].

For the 0% sample, the overall F_p profile did not visibly change post-irradiation (Fig. 13). $F_{p\,max}$ was not observed below 14 T in all 4 irradiated samples.

In all 4 APC-containing Cu-stabilised samples, the F_p profile curve did not clearly change post-irradiation, and $F_{p\,max}$ remained unobservable below 14 T (Figs. 14 and 15). However, in all 4 Ag-only samples, the F_p profile curvature increased to reveal a maximum and a decrease in F_p with increasing field, as $F_{p\,max}$ dramatically shifted to lower field strengths below 9 T. After 1 MGy irradiation, both the 7.5% and 15% Ag-only sample $F_{p\,max}$ peaks were found at higher field strengths than observed in the corresponding 1 kGy irradiated samples.

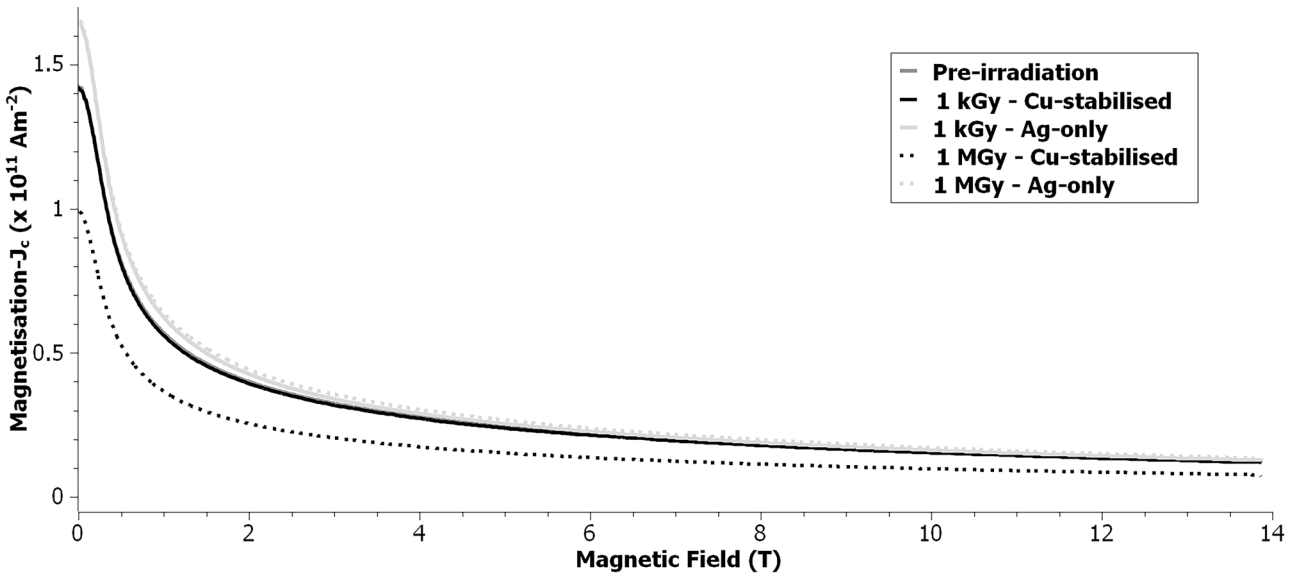

Fig. 7 Magnetisation critical current density versus magnetic field strength for the 0% Zr tape prior to gamma irradiation and the Cu-stabilised and Ag-only samples after 1 kGy and 1 MGy gamma irradiation—J_c values calculated at 20 K

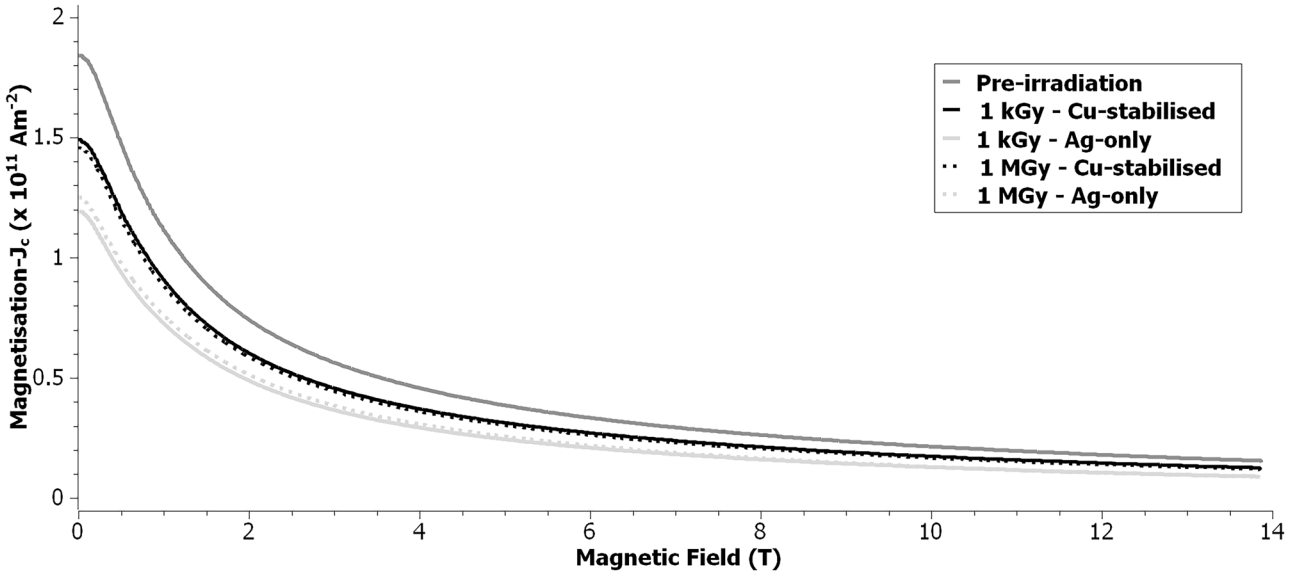

Fig. 8 Magnetisation critical current density versus magnetic field strength for the 7.5% Zr tape prior to gamma irradiation and the Cu-stabilised and Ag-only samples after 1 kGy and 1 MGy gamma irradiation—J_c values calculated at 20 K

The shift in $F_{p\,max}$ to lower field strengths below 9 T in the APC-containing Ag-only samples suggested that the onset of the overall pinning mechanism transition was occurring at greatly reduced fields after gamma irradiation. Previously, reduction in APC pinning energy has been accredited to irradiation-induced changes in coherence length [27]. The presence of APCs is also known to decrease the irradiation dose at which the transition in overall pinning mechanism occurs, leading to higher rates of degradation compared to non-APC tapes [7]. A gamma-induced transition to weak collective pinning by oxygen point defects present within the REBCO layer may explain the significant shift in $F_{p\,max}$ to lower field strengths. Collating this information, it would then make sense why the 15% Ag-only samples displayed lower $F_{p\,max}$ field strength peaks (after 1 kGy, 5.95 T; after 1 MGy, 6.4 T) relative to the analogous 7.5% samples (after 1 kGy, 6.1 T; after 1 MGy, 8 T). Though, the $F_{p\,max}$ shift to higher field strengths after the 1 MGy dose in both APC-containing samples was unexpected.

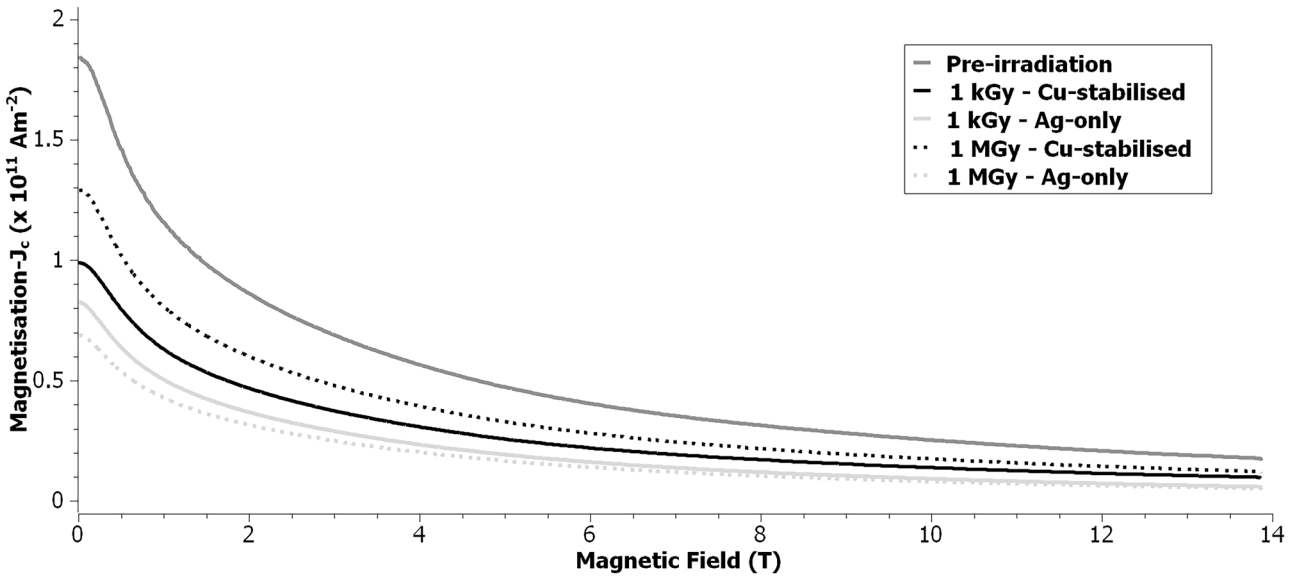

Fig. 9 Magnetisation critical current density versus magnetic field strength for the 15% Zr tape prior to gamma irradiation and the Cu-stabilised and Ag-only samples after 1 kGy and 1 MGy gamma irradiation—J_c values calculated at 20 K

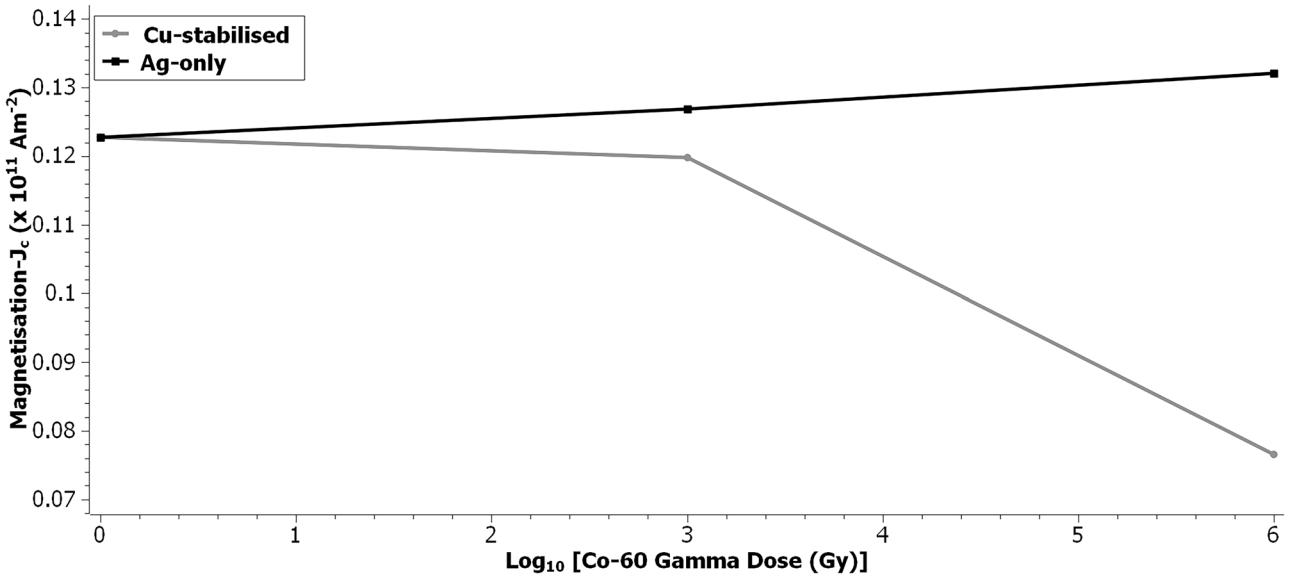

Fig. 10 Magnetisation critical current density values at 20 K and 13.85 T for the 0% Zr tape prior to gamma irradiation and the Cu-stabilised and Ag-only samples after 1 kGy and 1 MGy gamma irradiation

Considering the above observations in tandem with the work of Galstyan et al. [28], it was established that F_p versus field profiles can indeed probe irradiation-induced changes to the dominant pinning centre within the overall REBCO pinning landscape.

From these profiles, connections between the presence/absence of the Cu stabiliser and presence/absence of APCs on resulting $F_{p\,max}$ peak field strength shifts after gamma irradiation were noted. Removal of the two 20-μm thick Cu stabiliser layers in combination with the presence of APCs allowed gamma rays to alter the flux-pinning landscape, enabling the overall pinning mechanism transition onset at lower field strengths. The underlying cause of these observations is unclear.

3.1.3 Flux Creep Rate

Figures 16, 17, and 18 demonstrate the changes in calculated flux creep rates for the 3 sets of tape samples before

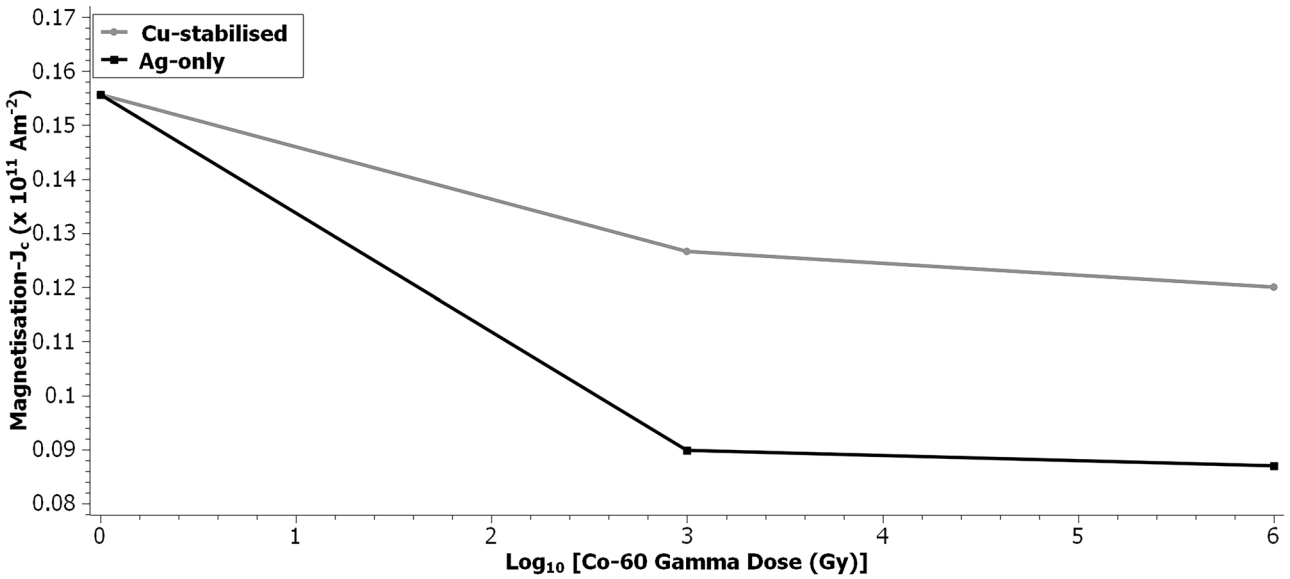

Fig. 11 Magnetisation critical current density values at 20 K and 13.85 T for the 7.5% Zr tape prior to gamma irradiation and the Cu-stabilised and Ag-only samples after 1 kGy and 1 MGy gamma irradiation

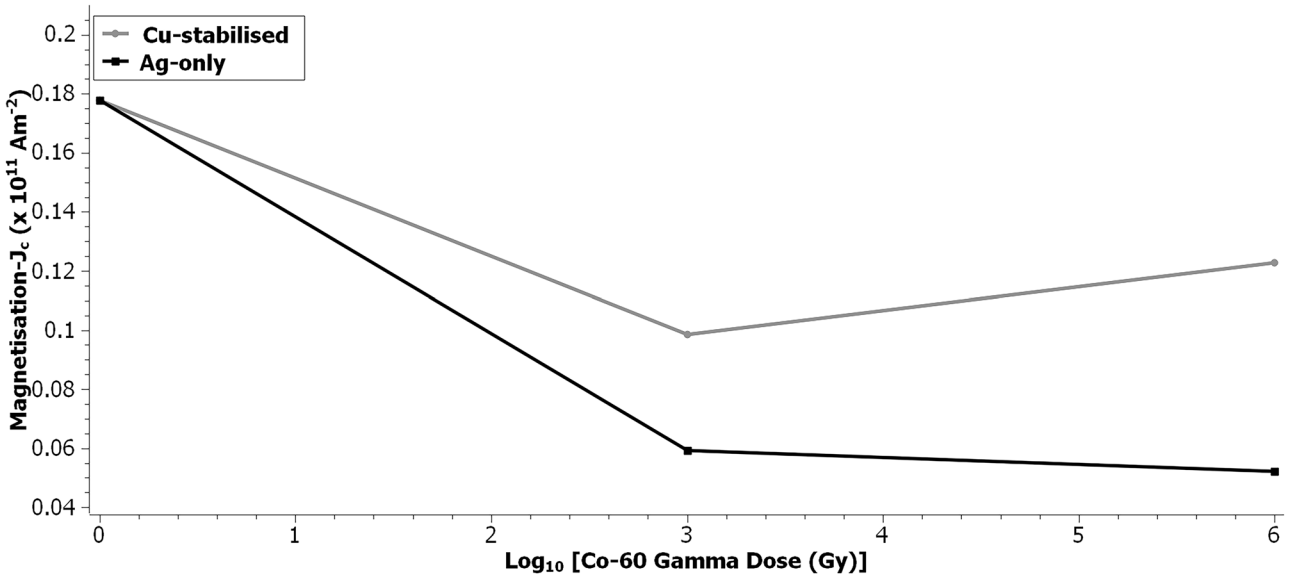

Fig. 12 Magnetisation critical current density values at 20 K and 13.85 T for the 15% Zr tape prior to gamma irradiation and the Cu-stabilised and Ag-only samples after 1 kGy and 1 MGy gamma irradiation

and after irradiation. Error values for the calculated creep rates were assumed to be the same as in Table 2.

For the 0% tape, flux creep rate decreased in all 4 samples post-irradiation. In the Cu-stabilised samples, creep rate was higher after 1 MGy than 1 kGy. In the Ag-only samples, flux creep rate decreased with increasing dose.

For the APC-containing tapes, flux creep rate increased in all 4 samples post-irradiation. It was noted that for each set of APC-containing samples, creep rate was lower after 1 MGy than 1 kGy.

Increasing radiation dose causes superconducting volume fraction and superfluid density to decrease, and both quantities are connected to J_c [4, 7, 10, 14, 15, 17–19]. Creep rate drastically decreased in the 0% Cu-stabilised 1 kGy irradiated sample, enabling minimal loss in J_c despite reduction in superconducting volume fraction/superfluid density (Fig. 10). Similar phenomena were seen in the APC-containing Cu-stabilised samples as dose increased from 1 kGy to 1 MGy, where the flux creep rate improved significantly, limiting

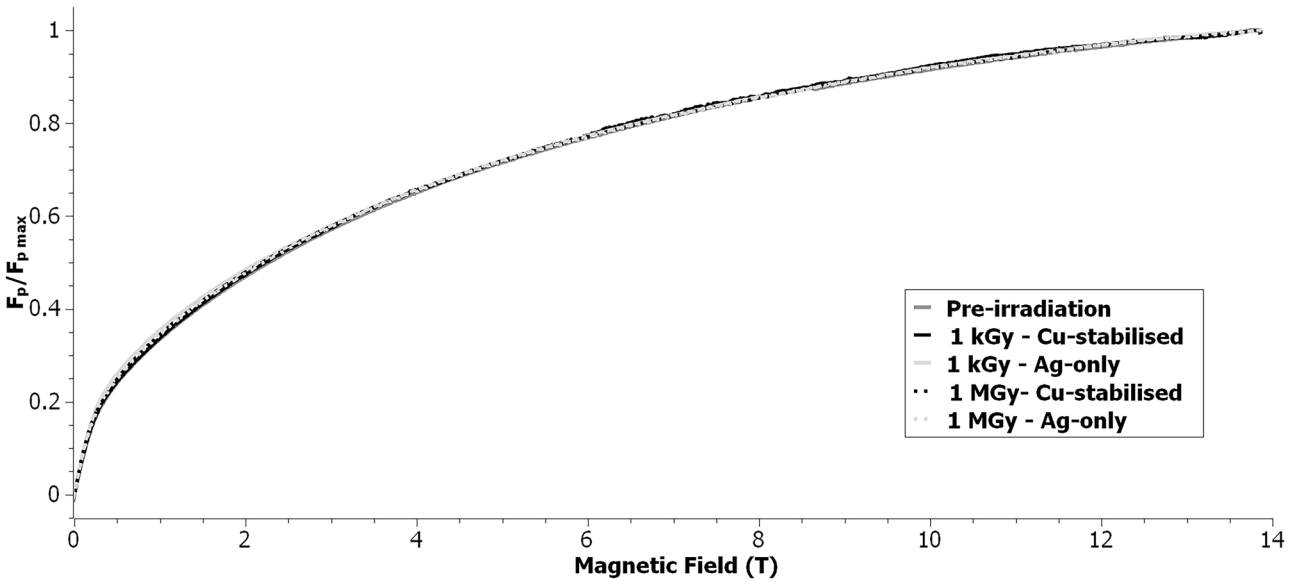

Fig. 13 Normalised pinning force versus magnetic field strength for the 0% Zr tape prior to gamma irradiation and the Cu-stabilised and Ag-only samples after 1 kGy and 1 MGy gamma irradiation—F_p values calculated at 20 K

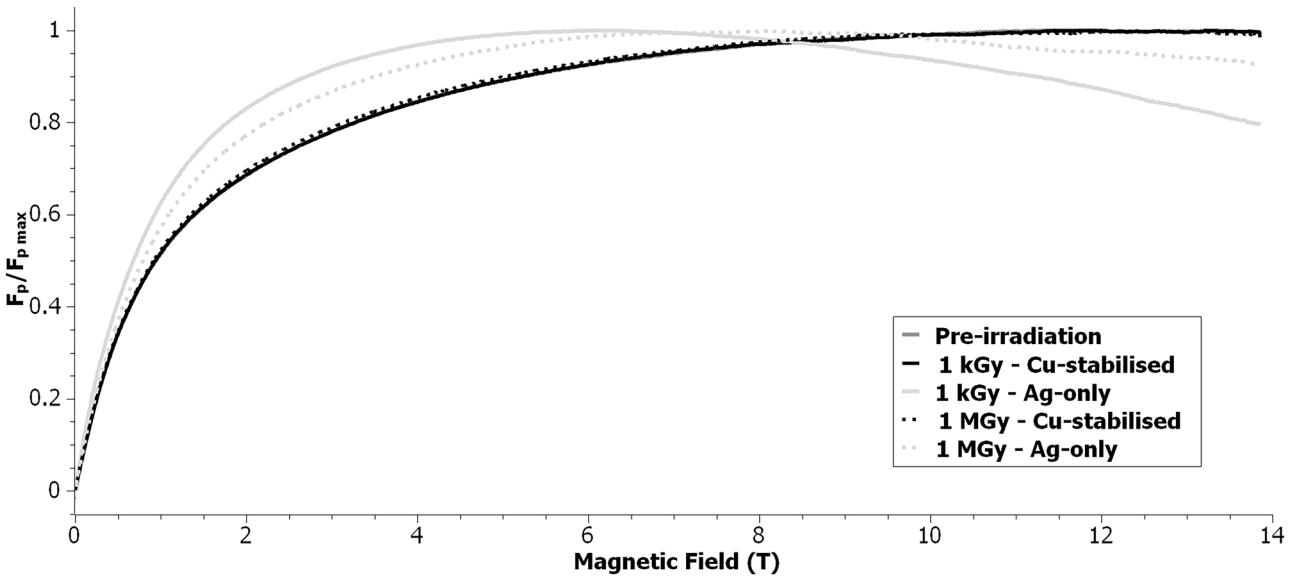

Fig. 14 Normalised pinning force versus magnetic field strength for the 7.5% Zr tape prior to gamma irradiation and the Cu-stabilised and Ag-only samples after 1 kGy and 1 MGy gamma irradiation—F_p values calculated at 20 K

further J_c degradation in the 7.5% sample and markedly increasing J_c in the 15% sample (Figs. 11 and 12).

Despite the lower rate of flux creep after 1 MGy irradiation in both APC-containing Ag-only samples, J_c decreased more relative to the 1 kGy irradiated samples. Considering the comparatively minor decreases in J_c and substantial decreases in flux creep rate after increasing dose to 1 MGy, it was suggested that a trade-off exists between superfluid density and flux creep rate affecting J_c after irradiation. This trade-off would also explain the heightened J_c in the 0% Ag-only samples with dose.

3.1.4 Summary

In a study by Eley et al., it was established that transitions in dominant pinning mechanism caused by irradiation, from strong individual pinning to weak collective pinning, increase flux creep rate and decrease J_c [27]. Combining the analyses

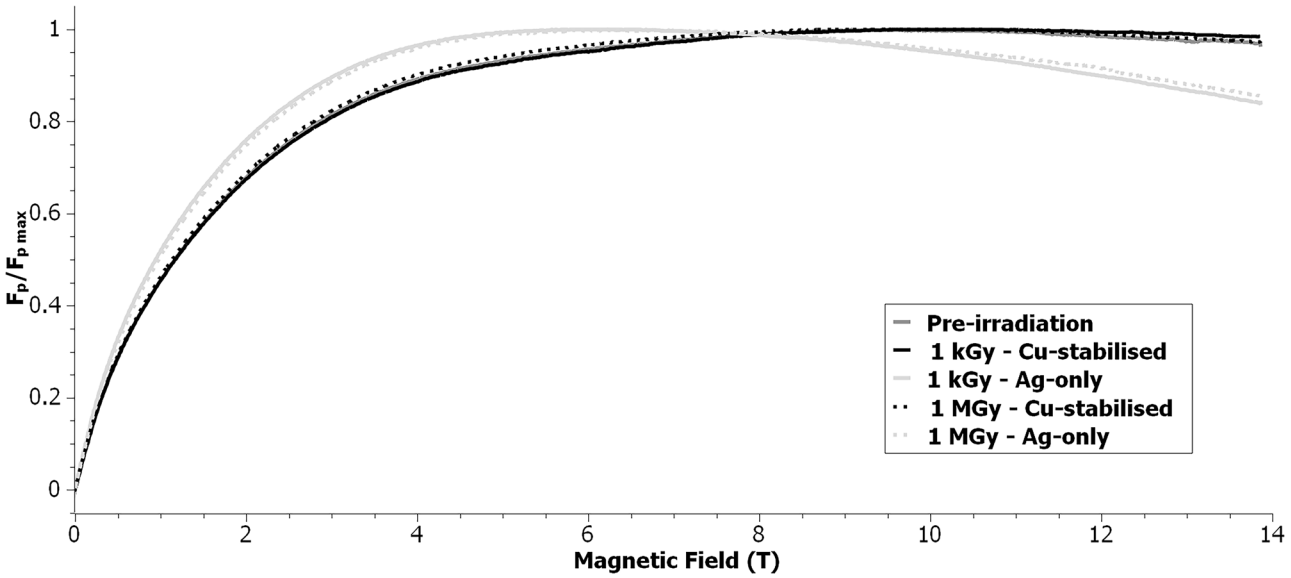

Fig. 15 Normalised pinning force versus magnetic field strength for the 15% Zr tape prior to gamma irradiation and the Cu-stabilised and Ag-only samples after 1 kGy and 1 MGy gamma irradiation—F_p values calculated at 20 K

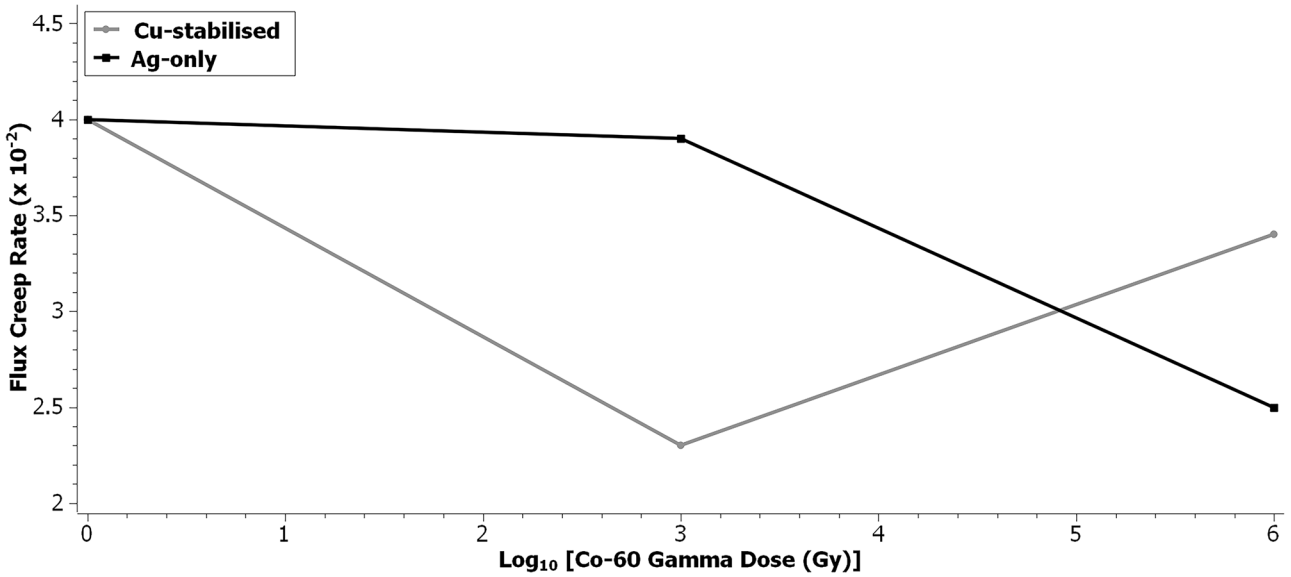

Fig. 16 Flux creep rates calculated at 20 K and 14 T for the 0% Zr tape prior to gamma irradiation and the Cu-stabilised and Ag-only samples after 1 kGy and 1 MGy gamma irradiation

on J_c, overall F_p, and flux creep rate changes post-irradiation, the conclusion was that flux-pinning landscapes were more susceptible to gamma-induced modifications when the Cu-stabiliser was removed, and APCs (in increasing concentration) were present.

Regardless of APC concentration, the rate of flux creep appeared to be the more important factor affecting performance in the balance between creep rate and superfluid density; the creep rate acts to either enhance J_c or prevent more dramatic J_c degradation as superfluid density universally decreases with irradiation. The resultant J_c after irradiation is thus dependent on pristine landscape and dose.

3.2 AC Magnetic Data

AC susceptibility measurements supplement the DC data by providing insight into changes in superfluid density via T_c [30], superconducting volume fraction via diamagnetic saturation [31], and overall F_p caused by the additional AC field via the irreversibility temperature (T_{irr}) [32]; T_{irr} is found

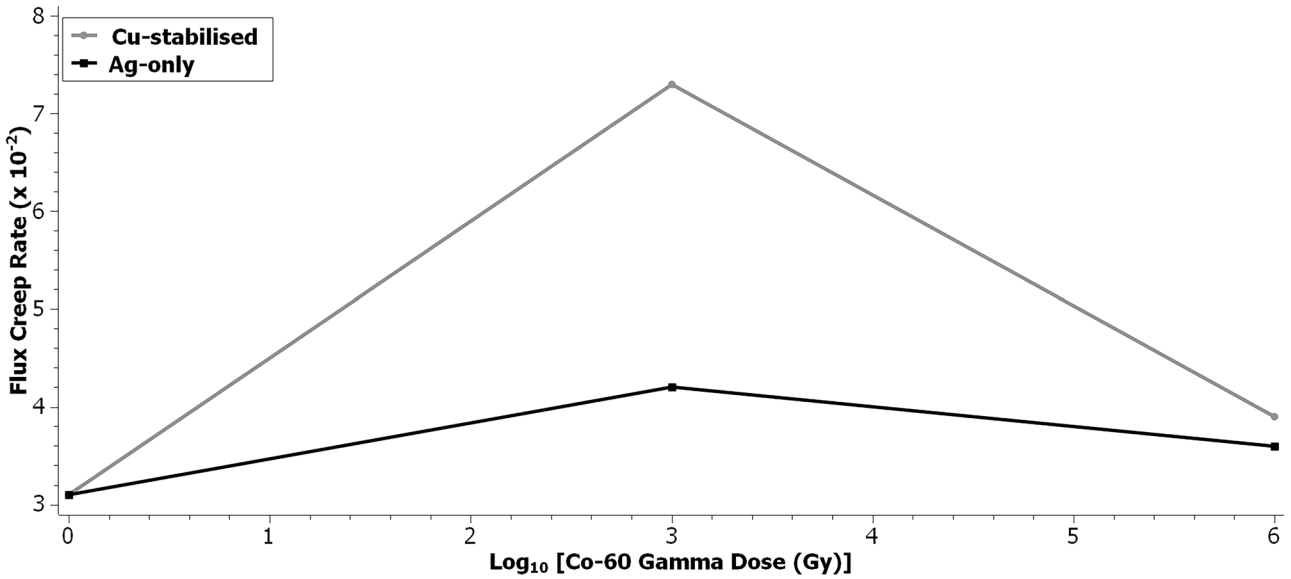

Fig. 17 Flux creep rates calculated at 20 K and 14 T for the 7.5% Zr tape prior to gamma irradiation and the Cu-stabilised and Ag-only samples after 1 kGy and 1 MGy gamma irradiation

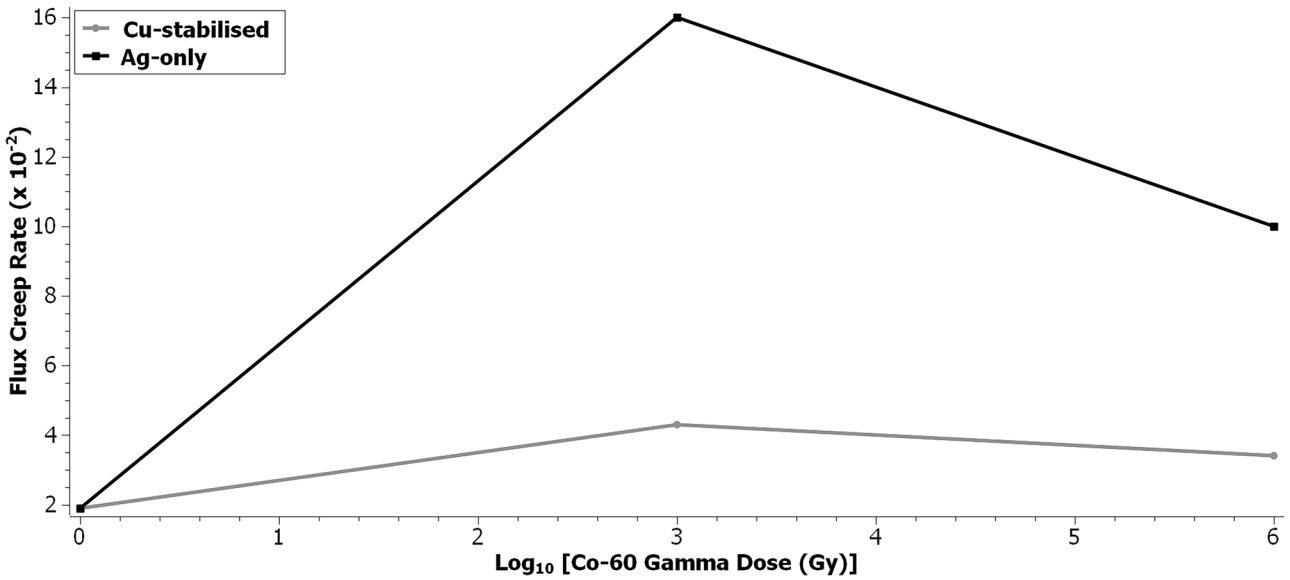

Fig. 18 Flux creep rates calculated at 20 K and 14 T for the 15% Zr tape prior to gamma irradiation and the Cu-stabilised and Ag-only samples after 1 kGy and 1 MGy gamma irradiation

from the imaginary component maximum. Both superfluid density and superconducting volume fraction relate to J_c, as discussed in Sect. 3.1.

Figure 19 shows the effect of increasing gamma dose on AC susceptibility in the 0% Cu-stabilised sample. With increasing gamma dose, T_c and diamagnetic saturation decreased, which was consistent with J_c changes observed in Fig. 10 and the proposed mechanisms behind those changes (improved flux creep rate relative to pristine sample counteracting reduction in superfluid density to maintain a decent superconducting volume fraction).

Figure 20 shows the influence of the Cu stabiliser on induced AC susceptibility changes in the 7.5% sample. In the 7.5% Cu-stabilised sample, there was negligible change in superfluid density, but a significant loss in superconducting volume fraction; for the analogous Ag-only sample, the opposite was true. Comparing flux creep rates in the 7.5% Cu-stabilised and Ag-only samples, creep rate was higher

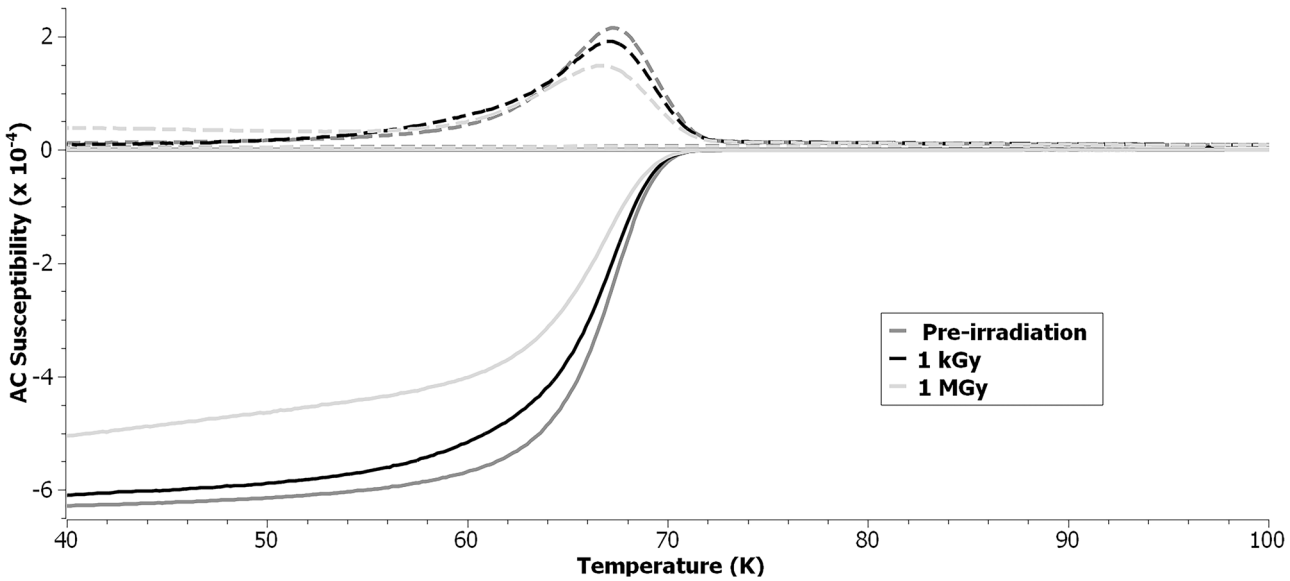

Fig. 19 AC susceptibility versus temperature for the 0% Zr tape prior to gamma irradiation and the Cu-stabilised samples after 1 kGy and 1 MGy gamma irradiation—susceptibility values at 14 T

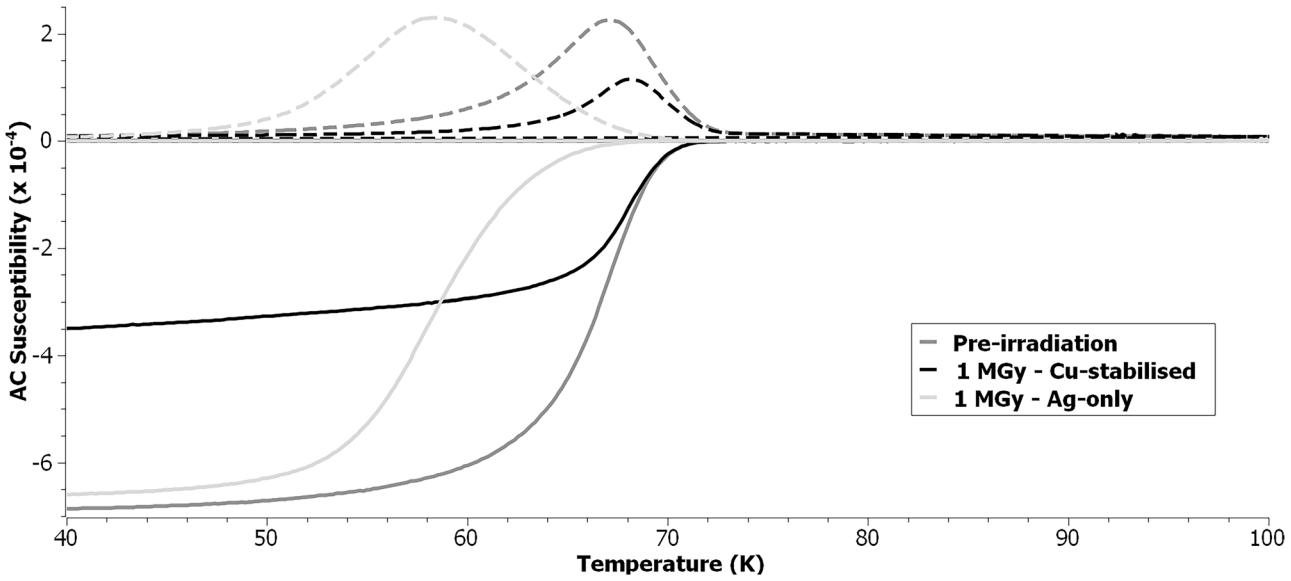

Fig. 20 AC susceptibility versus temperature for the 7.5% Zr tape prior to gamma irradiation and the Cu-stabilised and Ag-only samples after 1 MGy gamma irradiation—susceptibility values at 14 T

after irradiation when the stabiliser was present. These observations were consistent with the theorised rationale behind calculated J_c after 1 MGy irradiation in Fig. 11, where flux creep was the critical factor in the balance of parameters affecting J_c post-irradiation. Greater rates of flux motion under the AC drive field may explain the dramatic weakening of the diamagnetic signal in the Cu-stabilised sample.

Figure 21 shows the influence of the Cu stabiliser on induced AC susceptibility changes in the 15% sample. By comparison to the 7.5% sample, the 15% Cu-stabilised sample had a greater loss in superfluid density but lesser decrease in superconducting volume fraction. The lower flux creep rate in the 15% Cu-stabilised sample is perhaps what allowed for the relatively well-maintained post-irradiation high field J_c (Fig. 12), despite the lower superfluid density present. In the 15% Ag-only sample, higher flux creep rate and slightly reduced superfluid density were likely the cause of both lower J_c and diamagnetic saturation than observed in the 7.5% Ag-only sample. J_c and flux creep rate were also worse in the 15% Ag-only sample relative to the 15%

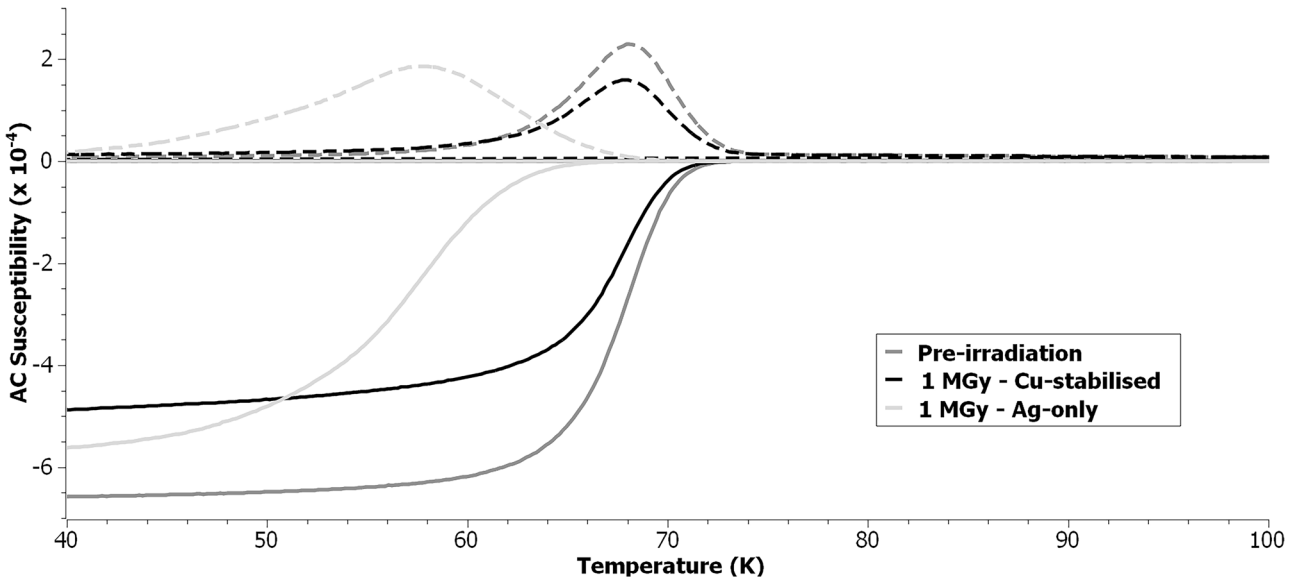

Fig. 21 AC susceptibility versus temperature for the 15% Zr tape prior to gamma irradiation and the Cu-stabilised and Ag-only samples after 1 MGy gamma irradiation—susceptibility values at 14 T

Cu-stabilised sample, possibly contributing to the smaller difference in saturation when compared to the analogous 7.5% sample profiles. The 15% Ag-only J_c at 14 T was only marginally smaller than the 7.5% Ag-only J_c value (as was superfluid density), indicative of the much higher flux creep rate relative to the 7.5% sample being the dominant factor leading to weakening of diamagnetic saturation.

The conclusion from magnetic data analysis is that reduction in superfluid density/superconducting volume fraction plays a role in performance degradation, but post-irradiation performance is more strongly dependent on how the rate of flux creep changes. For enhanced maintenance of maximal J_c under fusion-relevant conditions, minimisation of flux creep rate is the key.

4 Conclusion

The major conclusion from the magnetic data analysis discussed in this study is that flux creep is the performance limiting factor affecting REBCO coated conductor tapes at fusion-relevant temperatures and applied fields. At the tokamak magnet coil scale, flux creep manifests as AC losses, and AC losses have been identified as a primary issue hindering performance of the tapes in fusion.

The overall purpose of this work was to explore a novel approach towards understanding the evolution of REBCO tape performance under appropriate conditions for application in tokamaks. The use of multiple magnetic measurements on the same sample in a single experimental sequence, across different gamma-irradiated samples varying in APC concentration and presence/absence of the Cu-stabiliser, enabled the identification of flux creep as the universal problem affecting tape performance. The patterns in functional properties observed across each sample set post-irradiation were indicative of further investigation into gamma effects on tapes becoming a necessity in the future, bearing in mind the expected gamma flux on the magnets in tokamaks.

Moving forward beyond this study, the focus will be on implementation and verification of improvements to the tapes. The improvements themselves will be targeted towards reduction of irradiation-induced increases in flux creep rate and the lowering of flux creep rates generally in tapes. Enhanced prevention of flux creep/AC losses is desirable for any large-scale machine which employs superconductor technology [33], meaning this type of REBCO coated conductor tape development is transferable and would be beneficial more widely outside of tokamak research.

Acknowledgements We acknowledge the support of The University of Manchester's Dalton Cumbrian Facility (DCF), a partner in the National Nuclear User Facility, the EPSRC UK National Ion Beam Centre and the Henry Royce Institute. We recognise R. Edge for their assistance during the gamma irradiation experiments. The research used UKAEA's Materials Research Facility, which has been funded by and is part of the UK's National Nuclear User Facility and Henry Royce Institute for Advanced Materials. The authors would like to thank S. B. L. Chislett-McDonald, S. C. Wimbush, and A. London for their vital advice necessary for preparation of this article.

Funding This study was funded by the UKAEA Spherical Tokamak for Energy Production (STEP) programme Materials for STEP section within the Materials Business Unit.

Declarations

Competing Interests The authors declare no competing interests.

References

1. Bruzzone, P., Fietz, W.H., Minervini, J.V., Novikov, M., Yanagi, N., Zhai, Y., Zheng, J.: High temperature superconductors for fusion magnets. Nucl. Fusion **58**(10), 103001 (2018)
2. Lee, T.S., Jenkins, I., Surrey, E., Hampshire, D.P.: Optimal design of a toroidal field magnet system and cost of electricity implications for a tokamak using high temperature superconductors. Fusion Eng. Des. **98–99**, 1072–1075 (2015)
3. Windsor, C.G., Morgan, J.G.: Neutron and gamma flux distributions and their implications for radiation damage in the shielded superconducting core of a fusion power plant. Nucl. Fusion **57**, 116032 (2017)
4. Chudy, M., Eisterer, M., Weber, H.W., Veterníková, J., Sojak, S., Slugeň, V.: Point defects in $YBa_2Cu_3O_{7-x}$ studied using positron annihilation. Supercond. Sci. Technol. **25**(7), 075017 (2012)
5. Eisterer, M., Fuger, R., Chudy, M., Hengstberger, F., Weber, H.W.: Neutron irradiation of coated conductors. Supercond. Sci. Technol. **23**(1), 014009 (2009)
6. Prokopec, R., Fischer, D.X., Weber, H.W., Eisterer, M.: Suitability of coated conductors for fusion magnets in view of their radiation response. Supercond. Sci. Technol. **28**(1), 014005 (2014)
7. Fischer, D.X., Prokopec, R., Emhofer, J., Eisterer, M.: The effect of fast neutron irradiation on the superconducting properties of REBCO coated conductors with and without artificial pinning centers. Supercond. Sci. Technol. **31**, 044006 (2018)
8. Kutsukake, T., Somei, H., Ohki, Y., Nagasawa, K., Kaneko, F.: Gamma-irradiation effect on high-T_c superconductor $YBa_2Cu_3O_{7-x}$. Jpn. J. Appl. Phys **28**(Part 2, No. 8), L1393-L1394 (1989)
9. El-Hamalawy, A.A.E.-S., El-Zaidia, M.M., Ghali, E.A.: The effects of gamma-radiation on the high T_c superconductors $Er_1Ba_2Cu_3O_{7-\delta}$. Jpn. J. Appl. Phys **31**(Part 1, No. 11), 3529–3532 (1992)

10. Akduran, N.: Gamma irradiation effects on $EuBa_2Cu_3O_7$ high temperature superconductor. Radiat. Phys. Chem. **83**, 61–66 (2013)
11. Sekitani, T., Miura, N., Ikeda, S., Matsuda, Y.H., Shiohara, Y.: Upper critical field for optimally-doped $YBa_2Cu_3O_{7-\delta}$. Physica B **346–347**, 319–324 (2004)
12. Nikolo, M.: Flux dynamics in high-temperature superconductors. Supercond. Sci. Technol. **6**, 618 (1993)
13. Choi, W.J., Ahmad, D., Seo, Y.I., Ko, R.K., Kwon, Y.S.: Effect of the proton irradiation on the thermally activated flux flow in superconducting SmBCO coated conductors. Sci. Rep. **10**(1), 2017 (2020)
14. Egner, B., Geerk, J., Li, H.C., Linker, G., Meyer, O., Strehlau, B.: The influence of irradiation-induced defects on the superconductivity of $YBa_2Cu_3O_7$. Jpn. J. Appl. Phys. **26**(S3–3), 2141 (1987)
15. Antonova, L., Demikhov, T., Troitskii, A., Didyk, A., Kobzev, A., Yurasov, A., Samoilenkov, S., Mikhailova, G.: Effect of 2.5 MeV proton irradiation on the critical parameters of composite HTS tapes. Physica Status Solidi C **12**(1-2), 94–97 (2015)
16. Jia, Y., LeRoux, M., Miller, D.J., Wen, J.G., Kwok, W.K., Welp, U., Rupich, M.W., Li, X., Sathyamurthy, S., Fleshler, S., Malozemoff, A.P., Kayani, A., Ayala-Valenzuela, O., Civale, L.: Doubling the critical current density of high temperature superconducting coated conductors through proton irradiation. Appl. Phys. Lett. **103**(12), 122601 (2013)
17. Xiong, G.C., Li, H.C., Linker, G., Meyer, O.: Transport properties, phase transition, and recovery near 200 K of proton-irradiated $YBa_2Cu_3O_7$ thin films. Phys. Rev. B **38**(1), 240–243 (1988)
18. Shiraishi, K., Itoh, H., Yoda, O.: Electron irradiation effects on a $Ba_2YCu_3O_7$ superconductor. Jpn. J. Appl. Phys. **27**(Part 2, No. 12), L2339-L2341 (1988)
19. Hor, P.H., Bechtold, J., Xue, Y.Y., Chu, C.W., Hungerford, E.V., Maruyama, X.K., Backe, H., Buskirk, F.R., Connors, S.M., Jean, Y.C., Farmer, J.W.: Irradiation effects of flux pinning and J_c in high temperature superconductors. Physica C **185–189**, 2311–2312 (1991)
20. Hua, J., Welp, U., Schlueter, J., Kayani, A., Xiao, Z.L., Crabtree, G.W., Kwok, W.K.: Vortex pinning by compound defects in $YBa_2Cu_3O_{7-\delta}$. Phys. Rev. B **82**(2), 024505 (2010)
21. Matsushita, T., Isobe, G., Kimura, K., Kiuchi, M., Okayasu, S., Prusseit, W.: The effect of heavy ion irradiation on the critical current density in DyBCO coated conductors. Supercond. Sci. Technol. **21**(5), 054014 (2008)
22. Linden, Y., Iliffe, W.R., He, G., Danaie, M., Fischer, D.X., Eisterer, M., Speller, S.C., Grovenor, C.R.M.: Analysing neutron irradiation damage in $YBa_2Cu_3O_{7-x}$ high-temperature superconductor tapes. J. Microsc. **286**, 3–12 (2022)
23. Iliffe, W., Peng, N., Brittles, G., Bateman, R., Webb, R., Grovenor, C., Speller, S.: *In-situ* measurements of the effect of radiation damage on the superconducting properties of coated conductors. Superconductor Science and Technology **34**, 09LT01 (2021)
24. Superpower Furakawa, Superpower 2G HTS Coated Conductors. www.superpower-inc.com/content/2g-hts-wire (2013)
25. Seo, S., Noh, H., Li, N., Jiang, J., Tarantini, C., Shi, R., Jung, S., Oh, M. J., Liu, M., Lee J., Gu, G., Jung Jo, Y., Park, T., Hellstrom, E. E., Gao, P., Lee, S.: Artificially engineered nanostrain in $FeSe_xTe_{1-x}$ superconductor thin films for supercurrent enhancement. NPG Asia Materials **12**(7), (2020)
26. Ivan, I., Miu, D., Popa, S., Jakob, G., Miu, L.: On the determination of vortex creep parameters in superconductors using standard magnetization relaxation data. Supercond. Sci. Technol. **24**, 095005 (2011)
27. Eley, S., Leroux, M., Rupich, M.W., Miller, D.J., Sheng, H., Niraula, P.M., Kayani, A., Welp, U., Kwok, W.K., Civale, L.: Decoupling and tuning competing effects of different types of defects on flux creep in irradiated $YBa_2Cu_3O_{7-\delta}$ coated conductors. Supercond. Sci. Technol. **30**(1), 015010 (2016)
28. Galstyan, E., Pratap, R., Majkic, G., Kochat, M., Abraimov, D., Jaroszynski, J., Selvamanickam, V.: In-field critical current and pinning mechanisms at 4.2 K of Zr-added REBCO coated conductors. Superconductor Science and Technology **33**, 074007 (2020)
29. Putti, M., Vaglio, R., Rowell, J.: Radiation damaged MgB_2: a comparison with A15 superconductors. J. Phys. Conf. Ser. **97**, 012327 (2008)
30. Uemura, Y.J., Luke, G.M., Sternlieb, B.J., Brewer, J.H., Carolan, J.F., Hardy, W.N., Kadono, R., Kempton, J.R., Kiefl, R.F., Kreitzman, S.R., Mulhern, P., Riseman, T.M., Williams, D.L., Yang, B.X., Uchida, S., Takagi, H., Gopalakrishnan, J., Sleight, A.W., Subramanian, M.A., Chien, C.L., Cieplak, M.Z., Xiao, G., Lee, V.Y., Statt, B.W., Stronach, C.E., Kossler, W.J., Yu, X.H.: Universal correlations between T_c and n_s/m^* (carrier density over effective mass) in high T_c cuprate superconductors. Phys. Rev. Lett. **62**(19), 2317 (1989)
31. Srinivas, G., Howard, C.A., Bennington, S.M., Skipper, N.T., Ellerby, M.: Effect of hydrogenation on structure and superconducting properties of CaC_6. J. Mater. Chem. **19**, 5239 (2009)
32. Anderson, P.W., Kim, Y.B.: Hard superconductivity: theory of the motion of Abrikosov flux lines. Rev. Mod. Phys. **36**, 39 (1964)
33. Zhang, H., Wen, Z., Grilli, F., Gyftakis, K., Mueller, M.: Alternating current loss of superconductors applied to superconducting electrical machines. Energies **14**(8), 2234 (2021)